ACS chemical biology

pubs.acs.org/acschemicalbiology

Articles

SARS-CoV-2 RBD-Tetanus Toxoid Conjugate Vaccine Induces a Strong Neutralizing Immunity in Preclinical Studies

Yury Valdes-Balbin,*,■ Darielys Santana-Mederos,■ Lauren Quintero, Sonsire Fernández,■ Laura Rodriguez, Belinda Sanchez Ramirez,■ Rocmira Perez-Nicado, Claudia Acosta, Yanira Méndez, Manuel G. Ricardo, Tays Hernandez, Gretchen Bergado, Franciscary Pi, Annet Valdes, Tania Carmenate, Ubel Ramirez, Reinaldo Oliva, Jean-Pierre Soubal, Raine Garrido, Felix Cardoso, Mario Landys, Humberto Gonzalez, Mildrey Farinas, Juliet Enriquez, Enrique Noa, Anamary Suarez, Cheng Fang, Luis A. Espinosa, Yassel Ramos, Luis Javier González, Yanet Climent, Gertrudis Rojas, Ernesto Relova-Hernández, Yanelys Cabrera Infante, Sum Lai Losada, Tammy Boggiano, Eduardo Ojito, Kalet León, Fabrizio Chiodo, Françoise Paquet, Guang-Wu Chen,■ Daniel G. Rivera,■ Dagmar Garcia-Rivera,*,■ and Vicente Verez Bencomo*,■

Cite This: *ACS Chem. Biol.* 2021, 16, 1223−1233

Read Online

ACCESS | Metrics & More | Article Recommendations | Supporting Information

ABSTRACT: Controlling the global COVID-19 pandemic depends, among other measures, on developing preventive vaccines at an unprecedented pace. Vaccines approved for use and those in development intend to elicit neutralizing antibodies to block viral sites binding to the host's cellular receptors. Virus infection is mediated by the spike glycoprotein trimer on the virion surface via its receptor binding domain (RBD). Antibody response to this domain is an important outcome of immunization and correlates well with viral neutralization. Here, we show that macromolecular constructs with recombinant RBD conjugated to tetanus toxoid (TT) induce a potent immune response in laboratory animals. Some advantages of immunization with RBD-TT conjugates include a predominant IgG immune response due to affinity maturation and long-term specific B-memory cells. These result demonstrate the potential of the conjugate COVID-19 vaccine candidates and enable their advance to clinical evaluation under the name SOBERANA02, paving the way for other antiviral conjugate vaccines.

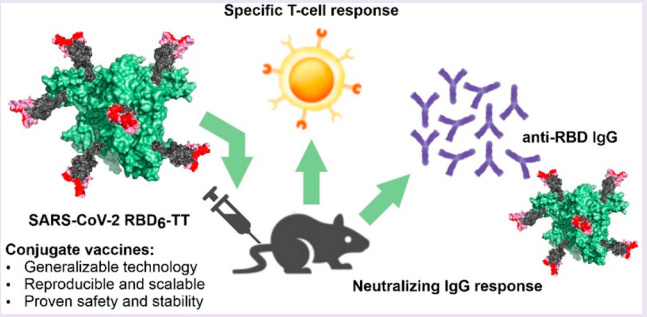

INTRODUCTION

The rapid development of preventive vaccines is crucial for controlling SARS-CoV-2 infection and ending the COVID-19 pandemic.[1] Viral infection is mediated by the initial binding of the receptor binding domain (RBD) of the spike (S)-glycoprotein trimer to the host's cell surface receptor, the angiotensin-converting enzyme 2 (ACE2).[2−5] Most of the 200 COVID-19 vaccines in development[6] aim to block this process.[1] By focusing on the whole S-protein or its RBD as an antigen, the primary goal is induction of anti-RBD antibodies that interfere with RBD-ACE2 interaction, blocking the first step of infection. Virus neutralization is mainly associated with antibodies against the receptor binding motif (RBM), a specific RBD region directly interacting with ACE2.[7] This type of antibody is not involved in antibody-dependent enhancement (ADE).[8]

Key advantages of the well-known recombinant subunit vaccine platform are their safety, stability at 2−8 °C, and facility to scale up the production.[9] While weak immunogenicity for a small recombinant protein such as the RBD (30 kDa) should be expected, typically requiring repeated vaccination,[10] it has been found that recombinant monomeric RBD (RBDm) in alum is sufficient to induce a neutralizing immune response in laboratory animals.[11] This has led to the clinical evaluation in humans of monomeric RBD-based vaccine candidates.[12] However, more recent reports have demonstrated a greater and higher quality immune response for larger RBD-containing macromolecular constructs.[13,14] In addition to its lower immunogenicity, recombinant RBDm

Received: April 11, 2021
Accepted: June 24, 2021
Published: July 4, 2021

https://doi.org/10.1021/acschembio.1c00272
ACS Chem. Biol. 2021, 16, 1223−1233

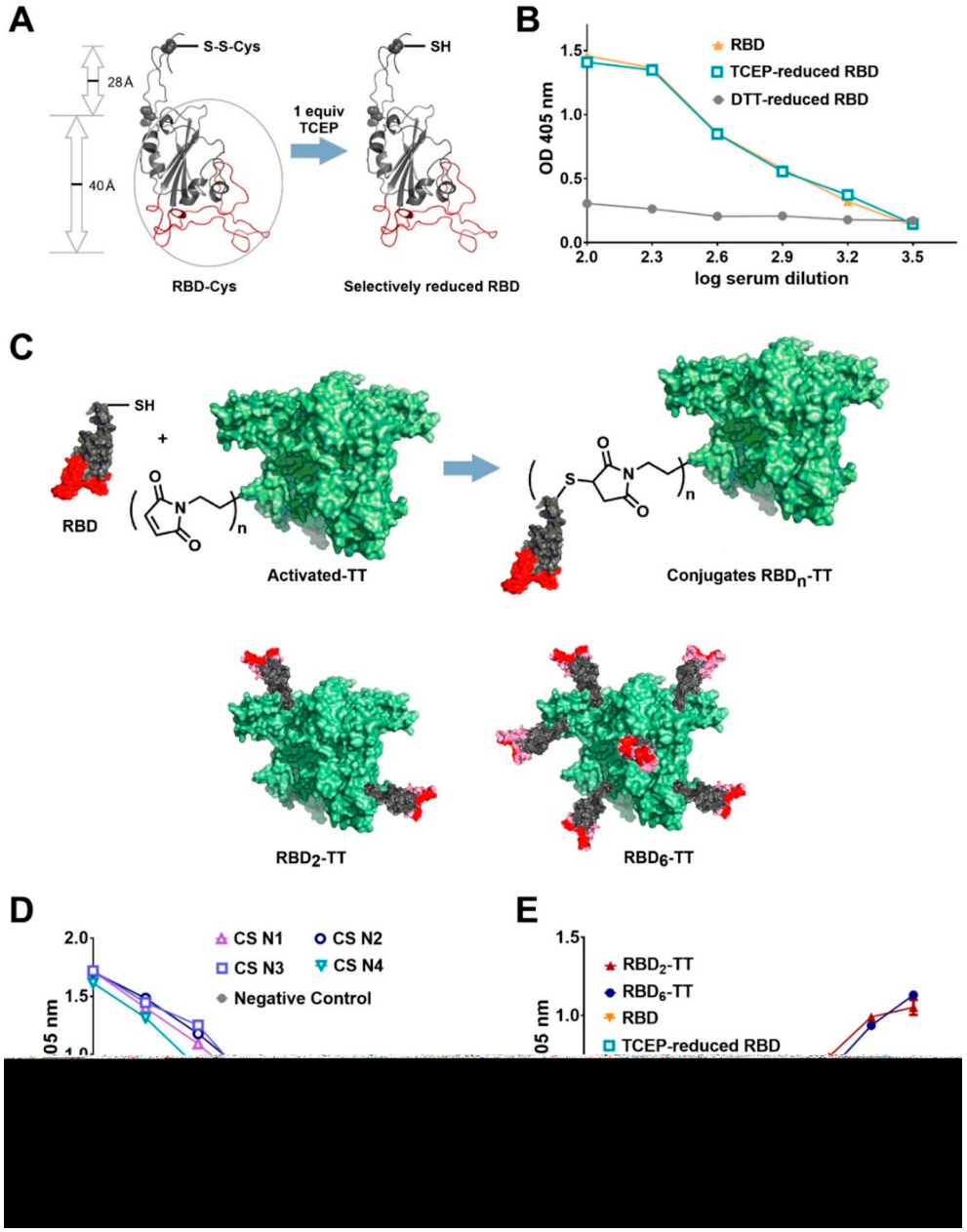

Figure 1. Synthesis of RBD-TT conjugates. (A) Selective reduction of the intermolecular disulfide bond at RBD Cys538 using TCEP. (B) Recognition of recombinant RBDm and reduced-RBD by a convalescent serum. (C) Conjugation of TCEP-reduced RBD to TT and representation of RBD_2-TT and RBD_6-TT conjugates. (D) Recognition of an RBD-BSA conjugate by four convalescent sera (CS), $n = 1-4$. (E) Binding of RBD_2-TT and RBD_6-TT conjugates to ACE2.

exposes to the immune system not only the critical RBM surface but also regions considered neo-epitopes, in the sense that they are not accessible in the S-glycoprotein at the virus surface.[13] Antibodies directed toward such neo-epitopes are expected to not bind the RBD at the surface of the virus, or to bind it with a low affinity, and therefore, turn out to be poorly functional. We hypothesized that the orientation of RBD, when conjugated to a large carrier like tetanus toxoid, exposes better the RBM surface, thereby likely increasing the level of neutralizing antibodies.[15−18]

The SARS-CoV-2 RBD comprises 195 amino acid residues, from Thr333 to Pro527, including the RBM 438−506 region that interacts directly with ACE2. This domain contains eight cysteine residues forming four disulfide bridges, three of them stabilizing the RBD core and one within the RBM.[6] Our recombinant RBD 319−541 was obtained in CHO cells (to preserve the mammalian glycosylation pattern) with an intentionally extended sequence adding S-glycoprotein residues 527 through 541 to include Cys538, which in the spike S-glycoprotein is connected to Cys590. The extended sequence includes two N-glycosylation sites at residues Asn331 and Asn343 and two O-glycosylation sites at Thr323 and Ser325. The selected sequence results in a protein expressed with an unpaired Cys538, to be used for chemical conjugation to the highly immunogenic carrier tetanus toxoid (TT). Here, we report a promising vaccine candidate based on a high-molecular-weight conjugate bearing several copies of recombinant RBD per unit of carrier protein. To our knowledge, the

https://doi.org/10.1021/acschembio.1c00272
ACS Chem. Biol. 2021, 16, 1223−1233

Figure 2. Immunogenicity evaluation. Immunization of BALB/c mice with RBD_2-TT/alum and RBD_6-TT/alum compared to RBDm/alum and RBD_2-TT. The serum of individual mice is represented by ▼ (RBDm/alum), ▲ (RBD_2-TT/alum), ♦ (RBD_2-TT or RBD_6-TT without alum), and ● (RBD_6-TT/alum). (A) Representation of the immunization protocol. (B) anti-RBD specific IgG on days 7, 14, 21, and 28. (C) Dose response to RBD_6-TT/alum on days 7, 14, 21, and 28. (D) Avidity index of antibodies elicited on day 28. The $p = 0.0047$ was calculated comparing only RDB_2-TT/alum and RBD_6-TT/alum. (E) RBD-specific IgG2a/IgG1 ratio. (F) anti-His tag antibodies compared to anti-RBD for RBD_6-TT.

immunogenic effect of conjugating the RBD to TT has not been assessed for SARS-CoV-2 or other coronaviruses. Previously, the SpyTag/SpyCatcher and enzymatic ligation technologies have been employed for the conjugation of RBD to self-assembled nanoparticles,[19−24] leading to highly immunogenic multivalent constructs. In our case, we relied on a scalable and reproducible chemical conjugation method for attaching the viral protein to a bacterial carrier. We demonstrate that RBD-TT conjugates induce a potent immune response in laboratory animals, paving the way for their evaluation in clinical trials.[25]

RESULTS AND DISCUSSION

Construction of RBD-TT Conjugates. Our design is based on the hypothesis that by conjugating several copies of the extended RBD to a large carrier protein, the resulting macromolecular construct is endowed with the multivalent RBD display required for a potent B-cell activation.[13,14] At the same time, the RBM would be well exposed (Figure 1, represented in red) and likely more available for immune recognition than other immunodominant epitopes present in the RBD core. To achieve this, a site-selective conjugation at an RBD residue spatially distant from the RBM is required, a process that should be reproducible and efficient on a large scale to allow a cost-effective vaccine production.

We expressed in CHO cells the recombinant RBD (Arg319-Phe541-$(His)_6$) bearing a flexible C-terminal fragment that includes unpaired Cys538, a residue distant from the RBM and suitable for conjugation. The inclusion of an additional free Cys538 in the extended RBD structure could jeopardize RBD folding due to potential disulfide (S−S) rearrangement with the other eight cysteine residues (scrambling). Nevertheless, we found that during fermentation, Cys538 either is spontaneously protected through an intermolecular S−S bond in an adduct with free cysteine present in the culture media or forms an RBD dimer that is separated from the monomer during purification. ESI-MS showed the presence of the four native S−S bonds, indicating a correctly folded RBD (see the Supporting Information, SI).

To achieve a site-selective conjugation, a key step is the selective reduction of the cysteinylated Cys538 to thiol-free without affecting the four S−S intramolecular bridges that maintain the native RBD conformation. After an extensive study of reaction conditions (i.e., time and stoichiometry of various reducing agents), we found that cysteinylated Cys538 could be selectively reduced to free thiol upon treatment with 1 equiv of tris(2-carboxyethyl)phosphine (TCEP) hydrochloride for 10 min without affecting the native conformation, as proven by recognition by a convalescent serum (Figure 1B) and ACE2 (Figure 1E). In contrast, RBD reduction with dithiothreitol (DTT) led to a complete loss of its recognition, suggesting a loss of the antigen's 3D structure (Figure 1B). To evaluate the integrity of the intramolecular disulfide bonds upon selective reduction of Cys538, we carried out a two-step experiment by reduction with 1 equiv of TCEP followed by incubation with 5 mM of *N*-ethylmaleimide (NEM) for 16 h at

https://doi.org/10.1021/acschembio.1c00272
ACS Chem. Biol. 2021, 16, 1223−1233

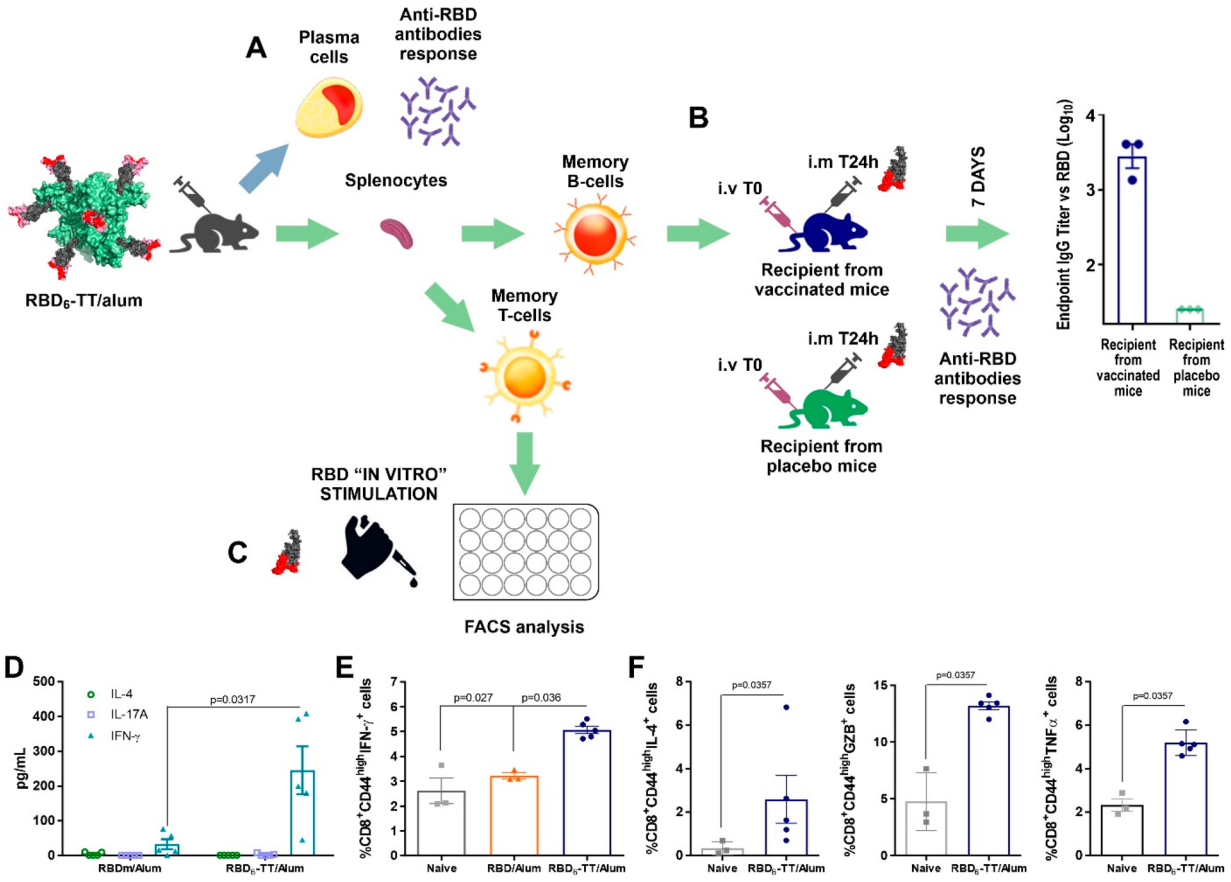

Figure 3. Memory B and T cells induced by RBD_6-TT. (A) Representation of the primary immune response to RBD_6-TT/alum (blue arrow). (B) Classical passive transfer of splenocytes from RBD_6-TT/alum-immunized BALB/c mice (up) and naïve mice (control, down) and stimulated with RBD/alum (up, strong secondary response on day 7 after immunization). (C) T-cell stimulation with RBD. (D) Cytokine secretion after *in vitro* RBD stimulation. (E) % RBD-specific memory T CD8+CD44highIFNγ+; (F) % RBD-specific memory T $CD_8^+CD_{44}^{high}IL\text{-}4^+$; % RBD-specific memory T $CD_8^+CD_{44}^{high}Granzyme^+$; % RBD-specific memory T $CD_8^+CD_{44}^{high}TNF_\alpha^+$.

4 °C (typical conjugation conditions). After deglycosylation with PNGase F, the derivatized RBD was digested with trypsin using an in-solution buffer-free digestion protocol.[26] The ESI-MS spectrum of the tryptic peptides corroborates NEM addition at Cys538, while the other four disulfide bonds were not noticeably affected (see the SI).

With the method for site-selective RBD derivatization in hand, we turned to obtain RBD-TT conjugates for immunogenicity evaluation. The conventional TT production is described in the SI, which renders a good manufacturing practice (GMP)-quality product with purity and stability adequate to be used as a carrier protein. We have been using TT as a carrier protein for carbohydrate−protein antibacterial conjugate vaccines for almost two decades, with millions of doses already applied.[27,28] The conjugation of thiol-functionalized antigens to maleimido-activated TT has been recently used to produce glycoconjugate vaccines,[29,30] with results of phase 1 in clinical evaluation reported.[31] The presence of multiple T- and B-cell epitopes of this highly immunogenic carrier[32] can potentiate cellular immunity when compared to the use of RBD alone. In addition, multimeric RBD-TT conjugates (RBD_n-TT) could simultaneously activate several B-cell receptors, thus enhancing B cell response.[13,14]

Considering the urgency to obtain at large scale a safe and effective, but also affordable, COVID-19 vaccine, we focused on the thiol-maleimide conjugation technology that has proven success in clinically validated conjugate vaccines.[27,31] To this end, TT was activated with approximately 20−30 maleimide groups per protein unit by treatment with *N*-succinimidyl 3-maleimidopropionate (SMP), followed by reactions with 2.5 or 10 equiv of TCEP-reduced RBD to produce conjugates bearing an average of 2 and 6 mol, respectively, of RBD per mol of TT (Figure 1C). The amount of RBD conjugated to TT was quantified in the crude reaction by size-exclusion HPLC (SE-HPLC), followed by purification to remove unreacted RBD. The RBD_2-TT and RBD_6-TT conjugates were obtained in 72% and 64% yield, respectively, and characterized by SDS-polyacrylamide gel electrophoresis (SDS-PAGE), SE-HPLC, dynamic light scattering (DLS), and ACE2 recognition assay. DLS indicated that the hydrodynamic diameter of RBD_6-TT is larger than that of RBD_2-TT, while both conjugates are larger than the carrier protein alone and its maleimide-activated form (Figure S9 and Table S3 in the SI). This is consistent with the SE-HPLC results. As TT is highly polydisperse (polydispersity index of 0.545), the resulting conjugates also show similar behavior.

Several batches of these conjugates were produced next under GMP at variable scales, with similar conjugation yield, notable reproducibility, and product stability proven, at least, over 6 months at 2−8 °C. As shown in Figure 1E, both conjugates recognize ACE2 slightly better than the original RBD, confirming the preservation of the RBD structure and the suitable exposition of RBM. As convalescent serum usually contains TT antibodies, we also prepared an RBD-bovine

https://doi.org/10.1021/acschembio.1c00272
ACS Chem. Biol. 2021, 16, 1223−1233

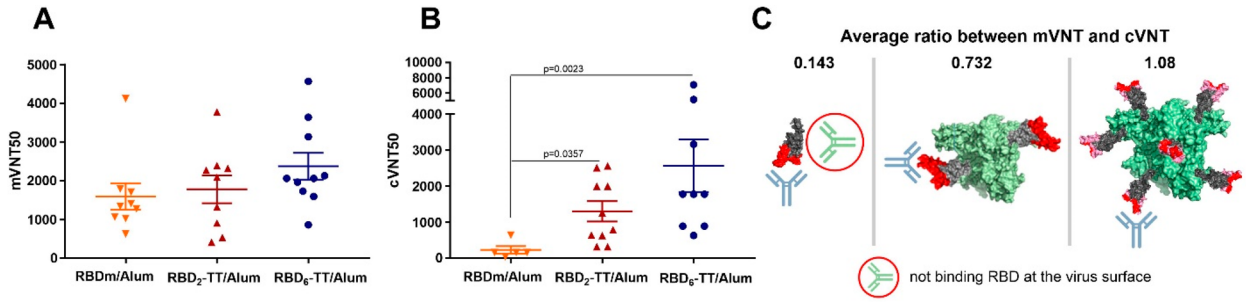

Figure 4. Virus neutralization by anti-RBD antibodies induced by RBDm and the RBD-TT conjugates on day 28. (A) $mVNT_{50}$ representing the serum dilution giving 50% inhibition of the ACE2−RBD interaction. (B) $cVNT_{50}$ measured as serum dilution giving 50% of virus neutralization. (C) $mVNT_{50}/cVNT_{50}$ ratio and a schematic representation of the different neutralizing IgG levels found for RBDm and the RBD-TT conjugates.

serum albumin (BSA) conjugate incorporating six RBD units per mole of BSA (RBD_6-BSA), which was recognized remarkably well by convalescent sera (Figure 1D). Collectively, these results demonstrate the conservation of RBD antigenic properties after site-selective carrier conjugation at Cys538 and the synthetic suitability of fine-tuning the number of RBD copies that can be incorporated onto the carrier to achieve the desired multivalent RBD display.

Animal Immunogenicity. IgG RBD-specific immune response in BALB/c mice was compared for RBD_6-TT/alum, RBD_2-TT/alum, RBDm/alum, and RBD_6-TT without alum. As shown in Figure 2, there was a strong immune response as proven by ELISA. On days 7 and 14 after the first immunization (T7 and T14, Figure 2C), RBD_6-TT/alum induced the highest level of anti-RBD antibodies. After the second dose at day 14, on days 21 and 28, all immunogens adsorbed in alum elicited higher anti-RBD IgG levels than without alum (T21 and 28, Figure 2C). The high and homogeneous early response for RBD_6-TT/alum could be an important asset for a vaccine in pandemic times. We explored the response to different dosages (0.5, 1, and 3 μg) of RBD_6-TT/alum and found a dose-dependent response at day 7. On day 14, before the second dose, the response was very high even for the lowest dosage (T14, Figure 2C).

We also compared affinity maturation of antibodies elicited by RBD_6-TT/alum and RBD_2-TT/alum with those elicited by RBD_2-TT and RBDm/alum. There was an increase in the avidity index (AI)[33] for antibodies induced by RBD_6-TT/alum (81%) and RBD_2-TT/alum (69%), which is consistent with a more pronounced affinity maturation and predicts a better antibody functionality (Figure 2D). Depending on the immunogen, the Th1/Th2 balance can be modulated, and as a result, it was also evaluated (Figure 2E). A biased Th2 immune response was observed for RBD_2-TT/alum (IgG2a/IgG1 ratio 0.54) and RBDm/alum (IgG2a/IgG1 ratio 0.40), while RBD_6-TT/alum displayed a more balanced Th1/Th2 immunity (IgG2a/IgG1 ratio 0.81). Although the His-tag is scarcely immunogenic, the effect in the immunogenicity of the His-tag at the RBD C-terminus needs to be evaluated. For this, ELISA plates were coated either with His-tag PDL2 protein or with RBDm and incubated for specific recognition in sera from mice immunized with RBD_6-TT. As shown in Figure 2F, sera recognized RBDm but not the PDL2 His-tag protein, indicating the absence of detectable antibodies against the His-tag.

COVID-19 vaccines are being evaluated in their capacity to protect the elderly,[34,35] and preclinical data should include evaluation in aged animals. For this purpose, elderly C57BL/6 mice were vaccinated with RBDm/alum, RBD_2-TT/alum, or RBD_6-TT/alum (Figure S10). After one dose, similarly high IgG titers were found for the conjugate immunogens, but after two doses (on day 28), significant differences were observed in IgG titers between animals immunized with RBD_6-TT/alum and those immunized with RBDm/alum or RBD_2-TT/alum at doses of 3 μg and 5 μg (Figure S10A). As determined by the molecular Virus Neutralization Test (mVNT50A), there is a significant difference in the functionality of antibodies elicited by RBD_6-TT/alum and RBD_2-TT/alum (Figure S10C). These results in elderly mice suggest that (a) the RBD_6-TT conjugate is a superior immunogen and (b) the two-dose immunization schedule is necessary to achieve a high quality anti-RBD IgG response.

Figure 3 shows the induction of RBD-specific memory B and T cells. Splenocytes taken on day 28 from mice immunized with two doses of RBD_6-TT/alum were intravenously transferred to naïve mice that were then boosted by a single dose of 3 μg RBDm/alum. In parallel, mice previously receiving splenocytes from placebo mice were primed with a single dose of 3 μg RBD/alum. As shown in Figure 3B, mice receiving splenocytes from RBD_6-TT/alum-immunized animals responded with a strong secondary RBD-specific IgG response (titers 10^3 to 10^4) after 7 days, while mice that received splenocytes from naïve donors showed a poor primary response. This experiment demonstrates the presence of RBD-specific memory B cells in the transferred splenocytes, which were able to be activated after a stimulus with RBDm/alum (here, a proxy to SARS-CoV-2 virus).

CD8+ T cells also play an important role in protection against SARS-CoV-2, as recently demonstrated.[36] To evaluate the specific T-cell response, we compared CD8+ T cells from RBD_6-TT/alum- and RBDm/alum-immunized mice. After *in vitro* RBD stimuli, splenocytes from mice immunized with RBD_6-TT/alum secreted higher levels of IFNγ compared to those immunized with RBDm/alum (Figure 3D). Flow cytometry showed a higher frequency of $CD8^+$ IFNγ-secreting cells (Figure 3E), suggesting a Th1 pattern, while IL-4 (characteristic of Th2 pattern) and IL-17A (characteristic of Th17 pattern) were not detected. The frequency of $CD8^+CD44^{high}$ memory T-lymphocytes producing IFN-γ, TNF-α, and Granzyme B increased significantly in RBD_6-TT/alum-immunized mice with respect to control mice (Figure 3F), indicating the relevant activation of cytotoxic T immune memory.

Antibody Functionality. We evaluated antibodies' ability to block the interaction between the virus and its receptor,[10] using $mVNT_{50}$[37] and the conventional Virus Neutralization

https://doi.org/10.1021/acschembio.1c00272
ACS Chem. Biol. 2021, 16, 1223−1233

Test ($cVNT_{50}$).[38] $mVNT_{50}$ evaluates the inhibition of the interaction between recombinant RBD and ACE2 at the molecular level, while at the cellular level, $cVNT_{50}$ evaluates inhibition of the interaction between the live virus and Vero E6 cells bearing ACE2 receptors. Antibodies resulting from Balb/c mice immunized with two doses of RBD_2-TT/alum and RBD_6-TT/alum were compared to antibodies elicited after immunization with RBDm/alum. $mVNT_{50}$ showed a high level of inhibition for all sera (Figure 4A), indicating that all tested antibodies displayed a similar efficacy in interfering with RBD−ACE2 interaction at the molecular level. On the other hand, $cVNT_{50}$ (Figure 4B) showed sharp differences between sera from animals immunized with RBD/alum and those immunized with the two conjugates. For RBDm/alum, the neutralization titer was 232, while for both conjugates there was a much higher level of virus neutralization, 1303 for RBD_2-TT and 2568 for RBD_6-TT. The $mVNT_{50}/cVNT_{50}$ ratio was 0.143, 0.732, and 1.08 for RBDm, RBD_2-TT, and RBD_6-TT, respectively. As depicted in Figure 4C, while antibodies neutralizing the virus are mainly directed to the RBM,[7,13] some elicited antibodies recognize other regions of monomeric RBD and, therefore, contribute to the $mVNT_{50}$ value in experiments with RBDm but probably do not recognize these RBD regions when they are camouflaged in the spike protein at the virus surface. We consider that the site-selective RBD conjugation to the large TT carrier can sterically shield those regions while leaving well-exposed the RBM, which helps increase the neutralizing IgG response (Figure 4).

CONCLUSIONS

We have demonstrated that the site-selective functionalization of the SARS-CoV-2 RBD followed by its chemical conjugation to a highly immunogenic carrier protein renders conjugates with the proper immunologically active RBD orientation, as proven by recognition studies. The extended RBD includes the well-exposed Cys538 at its C-terminal tail, placed distant enough from the key RBM region, so its conjugation to TT does not block the neutralizing RBM epitopes. However, Cys538 is not free in the expressed antigen, as the reactive thiol turned out to be capped with a Cys from the culture medium. Accordingly, the key step of this strategy was the selective reduction of the intermolecular S−S bond in the Cys538 adduct without affecting the four S−S bridges that preserve the antigenic RBD conformation.

An advantage of the conjugation technology here employed is the possibility to adjust the number of RBD units linked to the carrier. This proved to be relevant since RBD_6-TT elicited a superior immune response compared to RBD_2-TT, especially in the early response. The higher load of RBD in RBD_6-TT, compared to RBD_2-TT, might facilitate a suitable cross-linking of B-cell receptors,[13,14] which could contribute to the higher IgG response of the larger conjugate construction. We also proved that conjugation to TT led to a notable enhancement of the neutralizing response, probably due to the T helper effect of the carrier and the greater spatial accessibility of the RBM compared to other RBD regions. In humans, the TT-specific pre-existing T helper cells can contribute to antibody production after vaccination with RBD-TT conjugates.

On the basis of these results, various GMP batches of the vaccine candidates RBD_2-TT/alum and RBD_6-TT/alum were produced and absorbed on alum as final vaccine candidates. A phase I clinical trial[25] was initiated in October 2020, with interim results also confirming a better performance of a vaccine based on RBD_6-TT/alum. This vaccine candidate, named SOBERANA02, advanced in December 2020 to a phase II multicenter, adaptive clinical trial with 910 subjects.[39] Whereas phase I and II clinical trial results will be reported in due course, the encouraging interim data prompted moving forward to a phase III trial in March 2021.[40]

The resulting vaccine candidate composed of an RBD_6-TT conjugate, the first one developed in Latin America, has important advantages, such as (a) induction of strong IgG neutralizing antibody and specific T-cell responses, (b) the well-known safety record of this vaccine platform, which is being confirmed in our clinical trials, (c) its stability at 2−8 °C allowing an effective distribution, and (d) both the expression and conjugation technologies' ability to be adapted to existing production capacities available in many countries. Some of these advantages are a "must" for developing nations, in which not only the distribution chain but also the required recombinant and conjugation capacities are available for this vaccine technology but not for other platforms currently licensed. The results here shown open a venue of possibilities for the generalization of the conjugate vaccine technology for SARS-CoV-2 and other coronaviruses.

METHODS

Production of Monomeric RBD (Arg319-Phe541-$(His)_6$) Recombinant Protein. The coding sequence for RBD 319−541 fused to a C-terminal hexahistidine tag was optimized for mammalian cell expression (hamster, *Crycetulus grisesus*), using the online gene optimization tools provided by Eurofins (Germany). The resulting nucleotide sequence was assembled and amplified by PCR using gene fragments synthesized by Eurofins and oligonucleotides synthesized by the Center for Genetic Engineering and Biotechnology (CIGB, Cuba) and cloned into an intermediate vector containing a CMV promoter and mouse Ig VH signal sequence gene. The whole expression cassette was subsequently recloned into the lentiviral vector pL6WBlast, kindly provided by CIGB. HEK-293T cells were cotransfected with the lentiviral vector containing the gene of interest plus the mixture of auxiliary plasmids pLPI, pLPII, and pLP/VSV-G and used to produce lentiviral particles. CHO-K1 host cells were transduced with lentiviral particles and grown in 96 well plates in the presence of the selection drug blasticidine. Supernantants were screened for secretion of recombinant RBD by ELISA, and transduced cells showing the highest secretion levels were adapted to grow in suspension in serum-free medium (a mixture of PFHMII with a Center of Molecular Immunology's proprietary medium) with shaking. Recombinant RBD319−541 was purified from cell culture supernatant by immobilized metal affinity chromatography (IMAC) with Ni-NTA Sepharose. Monomeric RBD was then isolated by size exclusion chromatography using Superdex 200.

ESI-MS Analysis of Recombinant RBD. Before ESI-MS analysis, the purified recombinant RBDm (Arg319-Phe541-$(His)_6$) was deglycosylated with PNGase-F in the presence of N-ethylmaleimide (NEM). The ESI-MS spectrum showing the multiply charged ions (Figure S1A, SI) was deconvoluted. The experimental molecular mass of the most intense signal was 26981.82 Da, which is approximately 119 Da higher than expected (26863.07 Da), probably due to cysteinylation and the presence of an O-glycoform (HexNAc+Hex +SA2). Also, a low-abundance signal at 26690.73 Da agrees very well with the monomer cysteinylated and O-glycosylated with HexNAc +Hex+SA (26690.96 Da). This heterogeneity indicates the presence of two major O-glycoforms (HexNAc+Hex+SA2 and HexNAc+Hex +SA). The assignments for all signals (Figure S1B) are summarized in Table S1. The experimental molecular masses agree with the expected values considering four disulfide bonds, two Asn potential N-glycosylation sites transformed into Asp residues during the PNGase-F treatment, two major O-glycoforms (HexNAc+Hex+SA2 and HexNAc+Hex+SA), and cysteinylated Cys538. It was also

https://doi.org/10.1021/acschembio.1c00272
ACS Chem. Biol. 2021, 16, 1223−1233

observed that NEM was added partially at the N-terminal residue of the protein. The protein was digested with trypsin using the in-solution buffer-free digestion protocol[26] and analyzed by ESI-MS. The ESI-MS spectrum of the proteolytic peptides (Figure S2A and Table S2) summarizes the corresponding assignments. The four disulfide bonds (C336−C361, C379−C432, C391−C525, and C480−C488) present in the spike protein of SARS-CoV-2 were detected. The signal detected at m/z 475.20 (3+; Figure S1C, left panel) was assigned to the C-terminal peptide C538VNFHHHHHH547 containing cysteinylated Cys538 (Table S1). The MS/MS spectrum confirmed this assignment. In the same expanded region (m/z 468−483), a small signal at m/z 477.19 (3+) indicated a minor presence of the C-terminal peptide C538VNFHHHHHH547 modified with NEM at Cys538, indicating that only a tiny portion of the Cys538 thiol group was free, while the majority was cysteinylated and, as a consequence, unable to react with NEM.

Reduction of RBD-Cys Adduct to Obtain the RBD with Free Cys538. Recombinant RBDm (14 mL, 12 mg mL^{-1}, 5.6 μmol) in 35 mM PBS at pH 7.4 and 0.5 mM EDTA reacted with a freshly prepared solution of TCEP hydrochloride (1.6 mL, 1 mg mL^{-1}, 5.6 μmol, 1 equiv) for 10 min at RT. The conversion to the decysteinylated RBD was confirmed by ESI-MS analysis: an aliquote was deglycosylated with PNGase-F in the presence of 5 mM NEM and digested with trypsin as described above. The selective and efficient cleavage of the cysteinyl aduct and its conversion to free Cys538 was demonstrated by the disappearance of the previously detected signal at m/z 475.19, corresponding to (Cys538+Cys)3+, and the detection of the signal at m/z 477.19 (Figure S3C, right panel), assigned to (Cys538+NEM)3+. The other four disulfide bonds were not noticeably affected in the treatment with TCEP, as they were detected with similar intensities.

Activation of Tetanus Toxoid with Maleimide. A solution of tetanus toxoid (TT) (10 mL, 5 mg mL^{-1}, 50 mg, MW 150 kDa, 0.33 μmol) in 100 mM 4-(2-hydroxyethyl)piperazine-1-ethanesulfonic acid (HEPES) at pH 7.8 reacted with a freshly prepared solution of *N*-succinimidyl 3-maleimidopropionate in DMSO (187 μL, 75 mg mL^{-1}, 53 μmol, 160 equiv of SMP per mol of TT). The mixture was gently stirred for 1 h at RT, purified by diafiltration (100 kDa cutoff) with 35 mM PBS at pH 7.4 and 5 mM EDTA, and finally concentrated to 18 mg mL^{-1}, as measured by Lowry's method.[41] The stoichiometry of maleimide incorporated to TT was 20−30 maleimide groups/TT, as measured by a reversed Ellman method.[42]

Conjugation of RBD to Maleimide-Activated TT. Following the RBDm reduction procedure with TCEP, a solution of RBD with free Cys538 (13.5 mL, 12 mg mL^{-1}, 5.4 μmol) was treated with maleimide-activated TT (4.5 mL, 18 mg mL^{-1}, 0.54 μmol) in 35 mM PBS at pH 7.4 and 5 mM EDTA (final concentrations: RBD, 9 mg mL^{-1}; activated-TT, 4.5 mg mL^{-1}; molar ratio RBD/TT, 10:1). The reaction mixture was gently stirred for 16 h at 5 ± 3 °C. Cysteamine hydrochloride (0.6 mL, 5 mg mL^{-1}) was added, and the reaction was incubated for 30 min at RT. The amount of RBD incorporated into TT was monitored and quantified by the decrease in the SE-HPLC peak area for RBD. The average stoichiometry of RBD linked to TT was 6.4 (RBD_6-TT). Conjugate RBD_6-TT was obtained in 64% yield (based on RBD) after purification by diafiltration (100 kDa cutoff) with 20 washes of 1 mM phosphate buffer, at pH 7.0. Using the same conjugation procedure but with a nRBD/maleimide-activated TT molar ratio of 2.5:1, a conjugate was obtained in 72% yield with an average stoichiometry of 2 RBD per TT (RBD_2-TT). An RBD_6-BSA conjugate was also obtained in 92% from maleimide-activated BSA using the same protocol. The purified RBD-TT and RBD-BSA conjugates were characterized by SE-HPLC, SDS-PAGE, Western blot, and ELISA. The final products were tested using the kinetic LAL method; the acceptable limit for endotoxin content was set as 100 EU/mL. The purified RBD-TT and RBD-BSA conjugates were characterized by SE-HPLC, SDS-PAGE, Western blot, and ELISA. The final products were tested using the kinetic LAL method, and an upper limit for acceptable endotoxin was set at <100 EU/mL.

Animal Experiments. Immunogenicity of the RBD-TT conjugates and RBDm was evaluated in BALB/c mice (age: 6−8 weeks, 15−20 g) and elderly C57BL/6 mice (age: 66−68 weeks). All animals were supplied by the National Center for Laboratory Animals Breeding (CENPALAB), Havana, Cuba with their health certificates. All protocols were approved by the Finlay Vaccine Institute Ethical Committee.

Immunization Schedule and Sera Samples. Intramuscular injection on days 0 and 14; sera were collected at days 0 (before immunization) and at days 7, 14, 21 and 28.

Immunogenicity experiments included groups of 10 mice injected with (a) 3 μg of RBD-TT conjugates adjuvated with 500 μg of $Al(OH)_3$ or without adjuvant, (b) 3 μg of RBDm adjuvated with 500 μg of $Al(OH)_3$, and (c) 500 μg of $Al(OH)_3$ as a control. Dose−response experiment included groups of 10 mice immunized with 0.5, 1, or 3 μg of RBD_6-TT adjuvated with 500 μg of $Al(OH)_3$. Cytokine and T memory responses were evaluated in BALB/c mice immunized with 1 μg of RBD-TT conjugates adjuvated with 500 μg of $Al(OH)_3$.

Anti-RBD IgG ELISA. The 96 well ELISA plates (NUNC) were coated with 50 μL of RBD antigen at 3 μg mL^{-1} in carbonate-bicarbonate buffer at pH 9.6 for 1 h at 37 °C. Plates were blocked in 5% skim milk-PBS for 1 h at 37 °C. After five washes with PBS-0.5% Tween 20 (PBS-T), serum samples (diluted 1:3 v/v in PBS-1% BSA solution, pH 7.2) were added in serial dilution starting from 1/50. Plates were incubated for 1 h at 37 °C and washed with PBS-T. Goat antimouse IgG-HRP antibodies (Sigma-Aldrich) diluted 1/5000 in PBS-1% BSA pH 7.2) were added and incubated for 1 h at 37 °C. Following five washes with PBS-T, 3′,3′5,5′-tetramethylbenzidine (TMB) was added to the plates and incubated for 20 min. Reactions were stopped with 2 N H_2SO_4, and the absorbance was measured at 450 nm in a microplate reader ELISA Multiskan EX (ThermoScientific). The end point titer was defined as the highest reciprocal dilution of serum that gives an absorbance 4-fold greater than preimmune serum diluted 1/50.

Molecular Virus Neutralization Assays. The ability of anti-RBD specific antibodies to inhibit the RBD−ACE2 interaction was evaluated in a Molecular Virus Neutralization Assay. Briefly, microtiter plates (High binding, Costar) were coated with 50 μL/well of ACE2-mFc (5 μg mL^{-1}) in 0.1 M carbonate-bicarbonate buffer at pH 9.6 and incubated overnight at 4 °C. Plates were blocked with 200 μL/well of 2% NFDM/PBST for 1 h at 37 °C. Serial dilutions of individual sera were mixed 1:1 (v/v) with RBD-hFc (40 ng mL^{-1}) and incubated for 1 h at 37 °C. As a negative control, samples of sera from the placebo group mice were equally prepared. All samples were diluted in 0.2% NFDM/PBST (assay buffer). Mixtures were incubated for 2 h at 37 °C. Next, alkaline phosphatase-conjugated antihuman IgG antibody (1:1000, 50 μL/well) was added followed by incubation for 1 h at 37 °C. Finally, *p*-nitrophenylphosphate (Sigma; 1 mg mL^{-1} in diethanolamine buffer at pH 9.8) was added, and the plates were incubated at RT for 40 min. Absorbance at 405 nm was measured using a microwell system reader (Organon Teknica). All incubations were followed by three washing steps with PBST. Maximal recognition corresponds to RBD-hFc (40 ng mL^{-1}) mixed 1:1 (v/v) with assay buffer. The molecular viral neutralization titer ($mVNT_{50}$) represents the highest serum dilution giving 50% inhibition of maximal recognition. The serum dilutions were log transformed, and data were adjusted to a log(inhibitor) vs normalized response with variable slope nonlinear regression.

Virus Neutralization Assay. The virus neutralization assay was performed following the recommendation of Manenti et al.[38] with few modifications. Animal serum samples were heat-inactivated for 30 min at 56 °C. Two-fold serial dilutions of each sample serum (starting in 1:10 until 1:2560) were then mixed with an equal volume of viral suspension containing 100 median tissue culture infectious doses (TCID50) of SARS-CoV-2 (Strain 2025, Cuban Collection, National Laboratory of Civil Defense) and incubated for 1 h at 37 °C in a humidified atmosphere with 5% CO_2. After incubation, 100 μL of each dilution was added in duplicate to plates containing a semiconfluent VERO E6 monolayer (10^4 cell/well). The plates were incubated for 3 days at 37 °C in a humidified atmosphere with 5% CO_2. Then, the supernatant was carefully discarded, and 100 μL/well of a sterile PBS solution containing 0.02% neutral red (Sigma)

https://doi.org/10.1021/acschembio.1c00272
ACS Chem. Biol. 2021, 16, 1223−1233

was added. After 1 h of incubation at RT, the neutral red solution was discarded, and the cell monolayer was washed twice with sterile PBS-T. After the second incubation, PBS-T was carefully removed; then, 100 μL/well of a lysis solution (50 parts of absolute ethanol (Sigma), 49 parts of Milli-Q water, and one part of glacial acetic acid (Sigma) were added. Plates were incubated for 15 min at RT and then read at 540 nm in a spectrophotometer. The viral neutralizing titer 50 (VNT_{50}) is the highest serum dilution giving 50% of the average DO with respect to control cell wells (VERO E6 monolayer without mixture of virus-sera). In sera where VNT_{50} could not be calculated until 1:2560 dilution, the assay was repeated starting with a higher dilution.

Detection of RBD-Specific T Cells by Flow Cytometry. The RBD-specific memory T cells induced by the RBD_6-TT conjugate (mice immunized with 1 μg of RBD-TT conjugates adjuvated with 500 μg of $Al(OH)_3$) was determined by flow cytometry. Splenocytes from immunized or control mice were added to 24 well plates (3×10^6 splenocytes/well) and cultured for 72 h in RPMI medium 1640 (Gibco) supplemented with 10% (v/v) FBS (Capricorn), 100 U/mL penicillin-streptomycin, 1 mM pyruvate (Gibco), 50 μM β-mercaptoethanol, and 50 UI/ml IL-2 (Sigma-Aldrich). Mouse splenocytes were stimulated with 5 μg/mL of RBDm, and positive controls were stimulated with 5 μg/mL ConA (Sigma-Aldrich) for 24 h. Brefeldin A (10 μg/mL; BD Biosciences) was added 6 h before harvesting. Then, the cells were harvested and stained first with a live/dead fixable near-IR fluorescent dye (Invitrogen, Thermo Scientific), and anti-CD4 PerCP/Cy5.5 (RM4−5), anti-CD8 PE (S3−6.7), and anti-CD44 PE-cy7 (IM7) surface markers (eBiosciences) were added. Cells were subsequently fixed, permeabilized, and stained with anti-IFNγ FITC (XM61.2) and anti-IL-4 APC (11B11; eBiosciences). Flow cytometry data were acquired on a Gallios Cytometer (Beckman Coulter) and analyzed using Kaluza Software 1.2 version. CD4+ or CD8+ with CD44+ lymphocytes (defined as memory reactive RBD cells) were gated from live cells, and the percentage of IFN-γ+ and IL-4+ were recorded.

Quantification of Cytokines by ELISA. Cytokine secretion was quantified in the splenocyte supernatant from mice immunized with 1 μg of RBDm or RBD_6-TT adjuvated with 500 μg of $Al(OH)_3$, after *in vitro* stimulation with 5 μg/mL of RBDm. Supernatants were collected after 72 h of stimulation and stored at −80 °C. Cytokines in cell culture supernatants were quantified using an IFN-γ and IL-4 ELISA kit (Mabtech) according to the manufacturer's instruction.

Statistical Analysis. The analyses were performed with GraphPad Prism Software v.7.0.4. Two-sided nonparametric Mann−Whitney tests were conducted to compare differences between two experimental groups; Kruskal−Wallis ANOVA with Dunn's multiple comparisons tests were applied to compare more than two experimental groups. Antibody titer data were log transformed before analysis. P-values of <0.05 were considered significant.

■ ASSOCIATED CONTENT

Supporting Information

The Supporting Information is available free of charge at https://pubs.acs.org/doi/10.1021/acschembio.1c00272.

ESI-MS spectra, DLS, SE-HPLC chromatograms, and SDS-PAGE of the modified RBD and the RBD-TT conjugates; immunogenicity evaluation in elderly mice (PDF)

■ AUTHOR INFORMATION

Corresponding Authors

Yury Valdes-Balbin − *Finlay Vaccine Institute, Havana 11600, Cuba*; Email: yvbalbin@finlay.edu.cu

Dagmar Garcia-Rivera − *Finlay Vaccine Institute, Havana 11600, Cuba*; Email: dagarcia@finlay.edu.cu

Vicente Verez Bencomo − *Finlay Vaccine Institute, Havana 11600, Cuba*; orcid.org/0000-0001-5596-6847; Email: vicente.verez@finlay.edu.cu

Authors

Darielys Santana-Mederos − *Finlay Vaccine Institute, Havana 11600, Cuba*

Lauren Quintero − *Finlay Vaccine Institute, Havana 11600, Cuba*

Sonsire Fernández − *Finlay Vaccine Institute, Havana 11600, Cuba*

Laura Rodriguez − *Finlay Vaccine Institute, Havana 11600, Cuba*

Belinda Sanchez Ramirez − *Center of Molecular Immunology, Havana, Cuba*

Rocmira Perez-Nicado − *Finlay Vaccine Institute, Havana 11600, Cuba*

Claudia Acosta − *Finlay Vaccine Institute, Havana 11600, Cuba*

Yanira Méndez − *Laboratory of Synthetic and Biomolecular Chemistry, Faculty of Chemistry, University of Havana, Havana 10400, Cuba*; orcid.org/0000-0003-2124-4912

Manuel G. Ricardo − *Laboratory of Synthetic and Biomolecular Chemistry, Faculty of Chemistry, University of Havana, Havana 10400, Cuba*

Tays Hernandez − *Center of Molecular Immunology, Havana, Cuba*

Gretchen Bergado − *Center of Molecular Immunology, Havana, Cuba*

Franciscary Pi − *Center of Molecular Immunology, Havana, Cuba*

Annet Valdes − *Center of Molecular Immunology, Havana, Cuba*

Tania Carmenate − *Center of Molecular Immunology, Havana, Cuba*

Ubel Ramirez − *Finlay Vaccine Institute, Havana 11600, Cuba*

Reinaldo Oliva − *Finlay Vaccine Institute, Havana 11600, Cuba*

Jean-Pierre Soubal − *Finlay Vaccine Institute, Havana 11600, Cuba*

Raine Garrido − *Finlay Vaccine Institute, Havana 11600, Cuba*

Felix Cardoso − *Finlay Vaccine Institute, Havana 11600, Cuba*

Mario Landys − *Finlay Vaccine Institute, Havana 11600, Cuba*

Humberto Gonzalez − *Finlay Vaccine Institute, Havana 11600, Cuba*

Mildrey Farinas − *Finlay Vaccine Institute, Havana 11600, Cuba*

Juliet Enriquez − *National Civil Defense Research Laboratory, Mayabeque 32700, Cuba*

Enrique Noa − *National Civil Defense Research Laboratory, Mayabeque 32700, Cuba*

Anamary Suarez − *National Civil Defense Research Laboratory, Mayabeque 32700, Cuba*

Cheng Fang − *Shanghai Fenglin Glycodrug Promotion Center, Shanghai 200032, China*

Luis A. Espinosa − *Center for Genetic Engineering and Biotechnology, Havana 10600, Cuba*

Yassel Ramos − *Center for Genetic Engineering and Biotechnology, Havana 10600, Cuba;* orcid.org/0000-0003-3508-3830
Luis Javier González − *Center for Genetic Engineering and Biotechnology, Havana 10600, Cuba;* orcid.org/0000-0002-8875-3642
Yanet Climent − *Finlay Vaccine Institute, Havana 11600, Cuba*
Gertrudis Rojas − *Center of Molecular Immunology, Havana, Cuba*
Ernesto Relova-Hernández − *Center of Molecular Immunology, Havana, Cuba*
Yanelys Cabrera Infante − *Center of Molecular Immunology, Havana, Cuba*
Sum Lai Losada − *Center of Molecular Immunology, Havana, Cuba*
Tammy Boggiano − *Center of Molecular Immunology, Havana, Cuba*
Eduardo Ojito − *Center of Molecular Immunology, Havana, Cuba*
Kalet León − *Center of Molecular Immunology, Havana, Cuba*
Fabrizio Chiodo − *Finlay Vaccine Institute, Havana 11600, Cuba; Department of Molecular Cell Biology and Immunology, Amsterdam UMC, Vrije Universiteit Amsterdam, Amsterdam 1081HV, The Netherlands; Institute of Biomolecular Chemistry, National Research Council (CNR), Pozzuoli 80078 Napoli, Italy;* orcid.org/0000-0003-3619-9982
Françoise Paquet − *Centre de Biophysique Moléculaire, CNRS UPR 4301, F-45071 Orléans, Cedex 2, France;* orcid.org/0000-0001-8838-3445
Guang-Wu Chen − *Chengdu Olisynn Biotech. Co. Ltd., and State Key Laboratory of Biotherapy and Cancer Center, West China Hospital, Sichuan University, Chengdu 610041, People's Republic of China*
Daniel G. Rivera − *Laboratory of Synthetic and Biomolecular Chemistry, Faculty of Chemistry, University of Havana, Havana 10400, Cuba;* orcid.org/0000-0002-5538-1555

Complete contact information is available at: https://pubs.acs.org/10.1021/acschembio.1c00272

Author Contributions

■Y.V.-B., D.S.-M., S.F., B.S., G.-W.C., D.G.R., D.G.-R., and V.V.-B. contributed equally to this work.

Notes

The authors declare the following competing financial interest(s): Y.V.B., D.S.M, S.F., M.R., L.R., U.R., D.G.R., T.B., E.O., D.G.R., D.G.R., and V.V.B. are co-inventors on provisional SARS-CoV-2 vaccine patents (Cu 2020-69).

■ ACKNOWLEDGMENTS

We thank R. Pérez, L. Herrera, A. Lage, and E. Martinez (BioCubaFarma) for advice and support to the project; L. Castellanos for scientific advice and corrections; G. Reed for editing the English version; and E. Ramos for the figures' design. We are grateful to Fondo de Ciencia e Innovacion (FONCI, CITMA, Cuba) for financial support (Project-2020-20) and to the Leibniz Institute of Plant Biochemistry, Germany, for support in structural characterization.

■ REFERENCES

(1) Krammer, F. (2020) SARS-CoV-2 vaccines in development. *Nature 586*, 516−527.
(2) Chen, Y., Guo, Y., Pan, Y., and Zhao, Z. J. (2020) Structure analysis of the receptor binding of 2019-nCoV. *Biochem. Biophys. Res. Commun. 525*, 135−140.
(3) Shang, J., Ye, G., Shi, K., Wan, Y., Luo, C., Aihara, H., Geng, Q., Auerbach, A., and Li, F. (2020) Structural basis of receptor recognition by SARS-CoV-2. *Nature 581*, 221−224.
(4) Walls, A. C., Park, Y. J., Tortorici, M. A., Wall, A., McGuire, A. T., and Veesler, D. (2020) Structure, function, and antigenicity of the SARS-CoV-2 spike glycoprotein. *Cell 181*, 281−292.e6.
(5) Wan, Y., Shang, J., Graham, R., Baric, R. S., and Li, F. (2020) Receptor Recognition by the Novel Coronavirus from Wuhan: an Analysis Based on Decade-Long Structural Studies of SARS Coronavirus. *J. Virol. 94*, e00127−00120.
(6) Lan, J., Ge, J., Yu, J., Shan, S., Zhou, H., Fan, S., Zhang, Q., Shi, X., Wang, Q., Zhang, L., and Wang, X. (2020) Structure of the SARS-CoV-2 spike receptor-binding domain bound to the ACE2 receptor. *Nature 581*, 215−220.
(7) Piccoli, L., Park, Y. J., Tortorici, M. A., Czudnochowski, N., Walls, A. C., Beltramello, M., Silacci-Fregni, C., Pinto, D., Rosen, L. E., Bowen, J. E., Acton, O. J., Jaconi, S., Guarino, B., Minola, A., Zatta, F., Sprugasci, N., Bassi, J., Peter, A., De Marco, A., Nix, J. C., Mele, F., Jovic, S., Rodriguez, B. F., Gupta, S. V., Jin, F., Piumatti, G., Lo Presti, G., Pellanda, A. F., Biggiogero, M., Tarkowski, M., Pizzuto, M. S., Cameroni, E., Havenar-Daughton, C., Smithey, M., Hong, D., Lepori, V., Albanese, E., Ceschi, A., Bernasconi, E., Elzi, L., Ferrari, P., Garzoni, C., Riva, A., Snell, G., Sallusto, F., Fink, K., Virgin, H. W., Lanzavecchia, A., Corti, D., and Veesler, D. (2020) Mapping neutralizing and immunodominant sites on the SARS-CoV-2 spike receptor-binding domain by structure-guided high-resolution serology. *Cell 183*, 1024−1042.e21.
(8) Zang, J., Gu, C., Zhou, B., Zhang, C., Yang, Y., Xu, S., Bai, L., Zhang, R., Deng, Q., Yuan, Z., Tang, H., Qu, D., Lavillette, D., Xie, Y., and Huang, Z. (2020) Immunization with the receptor-binding domain of SARS-CoV-2 elicits antibodies cross-neutralizing SARS-CoV-2 and SARS-CoV without antibody-dependent enhancement. *Cell Discovery 6*, 61.
(9) Muhuri, M., and Gao, G. (2020) Is smaller better? Vaccine targeting recombinant receptor-binding domain might hold the key for mass production of effective prophylactics to fight the COVID-19 pandemic. *Signal Transduct. Target. Ther. 5*, 222.
(10) Jeyanathan, M., Afkhami, S., Smaill, F., Miller, M. S., Lichty, B. D., and Xing, Z. (2020) Immunological considerations for COVID-19 vaccine strategies. *Nat. Rev. Immunol. 20*, 615−632.
(11) Yang, J., Wang, W., Chen, Z., Lu, S., Yang, F., Bi, Z., Bao, L., Mo, F., Li, X., Huang, Y., Hong, W., Yang, Y., Zhao, Y., Ye, F., Lin, S., Deng, W., Chen, H., Lei, H., Zhang, Z., Luo, M., Gao, H., Zheng, Y., Gong, Y., Jiang, X., Xu, Y., Lv, Q., Li, D., Wang, M., Li, F., Wang, S., Wang, G., Yu, P., Qu, Y., Yang, L., Deng, H., Tong, A., Li, J., Wang, Z., Yang, J., Shen, G., Zhao, Z., Li, Y., Luo, J., Liu, H., Yu, W., Yang, M., Xu, J., Wang, J., Li, H., Wang, H., Kuang, D., Lin, P., Hu, Z., Guo, W., Cheng, W., He, Y., Song, X., Chen, C., Xue, Z., Yao, S., Chen, L., Ma, X., Chen, S., Gou, M., Huang, W., Wang, Y., Fan, C., Tian, Z., Shi, M., Wang, F.-S., Dai, L., Wu, M., Li, G., Wang, G., Peng, Y., Qian, Z., Huang, C., Lau, J. Y.-N., Yang, Z., Wei, Y., Cen, X., Peng, X., Qin, C., Zhang, K., Lu, G., and Wei, X. (2020) A vaccine targeting the RBD of the S protein of SARS-CoV-2 induces protective immunity. *Nature 586*, 572−577.
(12) Kashte, S., Gulbake, A., El-Amin, S. F., III, and Gupta, A. (2021) COVID-19 vaccines: rapid development, implications, challenges and future prospects. *Hum. Cell 34*, 711−733.
(13) Valdes-Balbin, Y., Santana-Mederos, D., Paquet, F., Fernandez, S., Climent, Y., Chiodo, F., Rodríguez, L., Sanchez Ramirez, B., Leon, K., Hernandez, T., Castellanos-Serra, L., Garrido, R., Chen, G.-W., Garcia-Rivera, D., Rivera, D. G., and Verez-Bencomo, V. (2021) Molecular Aspects Concerning the Use of the SARS-CoV-2 Receptor

Binding Domain as a Target for Preventive Vaccines. *ACS Cent. Sci. 7*, 757−767.
(14) Walls, A. C., Fiala, B., Schafer, A., Wrenn, S., Pham, M. N., Murphy, M., Tse, L. V., Shehata, L., O'Connor, M. A., Chen, C., Navarro, M. J., Miranda, M. C., Pettie, D., Ravichandran, R., Kraft, J. C., Ogohara, C., Palser, A., Chalk, S., Lee, E. C., Guerriero, K., Kepl, E., Chow, C. M., Sydeman, C., Hodge, E. A., Brown, B., Fuller, J. T., Dinnon, K. H., 3rd, Gralinski, L. E., Leist, S. R., Gully, K. L., Lewis, T. B., Guttman, M., Chu, H. Y., Lee, K. K., Fuller, D. H., Baric, R. S., Kellam, P., Carter, L., Pepper, M., Sheahan, T. P., Veesler, D., and King, N. P. (2020) Elicitation of potent neutralizing antibody responses by designed protein nanoparticle vaccines for SARS-CoV-2. *Cell 183*, 1367−1382.e17.
(15) Brouwer, P. J. M., Caniels, T. G., van der Straten, K., Snitselaar, J. L., Aldon, Y., Bangaru, S., Torres, J. L., Okba, N. M. A., Claireaux, M., Kerster, G., Bentlage, A. E. H., van Haaren, M. M., Guerra, D., Burger, J. A., Schermer, E. E., Verheul, K. D., van der Velde, N., van der Kooi, A., van Schooten, J., van Breemen, M. J., Bijl, T. P. L., Sliepen, K., Aartse, A., Derking, R., Bontjer, I., Kootstra, N. A., Wiersinga, W. J., Vidarsson, G., Haagmans, B. L., Ward, A. B., de Bree, G. J., Sanders, R. W., and van Gils, M. J. (2020) Potent neutralizing antibodies from COVID-19 patients define multiple targets of vulnerability. *Science 369*, 643−650.
(16) Rogers, T. F., Zhao, F., Huang, D., Beutler, N., Burns, A., He, W. T., Limbo, O., Smith, C., Song, G., Woehl, J., Yang, L., Abbott, R. K., Callaghan, S., Garcia, E., Hurtado, J., Parren, M., Peng, L., Ramirez, S., Ricketts, J., Ricciardi, M. J., Rawlings, S. A., Wu, N. C., Yuan, M., Smith, D. M., Nemazee, D., Teijaro, J. R., Voss, J. E., Wilson, I. A., Andrabi, R., Briney, B., Landais, E., Sok, D., Jardine, J. G., and Burton, D. R. (2020) Isolation of potent SARS-CoV-2 neutralizing antibodies and protection from disease in a small animal model. *Science 369*, 956−963.
(17) Yuan, M., Liu, H., Wu, N. C., Lee, C. D., Zhu, X., Zhao, F., Huang, D., Yu, W., Hua, Y., Tien, H., Rogers, T. F., Landais, E., Sok, D., Jardine, J. G., Burton, D. R., and Wilson, I. A. (2020) Structural basis of a shared antibody response to SARS-CoV-2. *Science 369*, 1119−1123.
(18) Zost, S. J., Gilchuk, P., Case, J. B., Binshtein, E., Chen, R. E., Nkolola, J. P., Schafer, A., Reidy, J. X., Trivette, A., Nargi, R. S., Sutton, R. E., Suryadevara, N., Martinez, D. R., Williamson, L. E., Chen, E. C., Jones, T., Day, S., Myers, L., Hassan, A. O., Kafai, N. M., Winkler, E. S., Fox, J. M., Shrihari, S., Mueller, B. K., Meiler, J., Chandrashekar, A., Mercado, N. B., Steinhardt, J. J., Ren, K., Loo, Y. M., Kallewaard, N. L., McCune, B. T., Keeler, S. P., Holtzman, M. J., Barouch, D. H., Gralinski, L. E., Baric, R. S., Thackray, L. B., Diamond, M. S., Carnahan, R. H., and Crowe, R. H., Jr. (2020) Potently neutralizing and protective human antibodies against SARS-CoV-2. *Nature 584*, 443−449.
(19) Ma, X., Zou, F., Yu, F., Li, R., Yuan, Y., Zhang, Y., Zhang, X., Deng, J., Chen, T., Song, Z., Qiao, Y., Zhan, Y., Liu, J., Zhang, J., Zhang, X., Peng, Z., Li, Y., Lin, Y., Liang, L., Wang, G., Chen, Y., Chen, Q., Pan, T., He, X., and Zhang, H. (2020) Nanoparticle vaccines based on the receptor binding domain (RBD) and heptad repeat (HR) of SARS-CoV-2 elicit robust protective immune responses. *Immunity 53*, 1315−1330.e9.
(20) Fougeroux, C., Goksøyr, L., Idorn, M., Soroka, V., Myeni, S. K., Dagil, R., Janitzek, C. M., Søgaard, M., Aves, K.-L., Horsted, E. W., Erdoğan, S. M., Gustavsson, T., Dorosz, J., Clemmensen, S., Fredsgaard, L., Thrane, S., Vidal-Calvo, E. E., Khalifé, P., Hulen, T. M., Choudhary, S., Theisen, M., Singh, S. K., Garcia-Senosiain, A., Van Oosten, L., Pijlman, G., Hierzberger, B., Domeyer, T., Nalewajek, B. W., Strøbæk, A., Skrzypczak, M., Andersson, L. F., Buus, S., Buus, A. S., Christensen, J. P., Dalebout, T. J., Iversen, K., Harritshøj, L. H., Mordmüller, B., Ullum, H., Reinert, L. S., de Jongh, W. A., Kikkert, M., Paludan, S. R., Theander, T. G., Nielsen, M. A., Salanti, A., and Sander, A. F. (2021) Capsid-like particles decorated with the SARS-CoV-2 receptor-binding domain elicit strong virus neutralization activity. *Nat. Commun. 12*, 324.
(21) Cohen, A. A., Gnanapragasam, P. N. P., Lee, Y. E., Hoffman, P. R., Ou, S., Kakutani, L. M., Keeffe, J. R., Wu, H. J., Howarth, M., West, A. P., Barnes, C. O., Nussenzweig, M. C., and Bjorkman, P. J. (2021) Mosaic nanoparticles elicit cross-reactive immune responses to zoonotic coronaviruses in mice. *Science 371*, 735−741.
(22) Saunders, K. O., Lee, E., Parks, R., Martinez, D. R., Li, D., Chen, H., Edwards, R. J., Gobeil, S., Barr, M., Mansouri, K., Alam, S. M., Sutherland, L. L., Cai, F., Sanzone, A. M., Berry, M., Manne, K., Bock, K. W., Minai, M., Nagata, B. M., Kapingidza, A. B., Azoitei, M., Tse, L. V., Scobey, T. D., Spreng, R. L., Rountree, R. W., DeMarco, C. T., Denny, T. N., Woods, C. W., Petzold, E. W., Tang, J., Oguin, T. H., Sempowski, G. D., Gagne, M., Douek, D. C., Tomai, M. A., Fox, C. B., Seder, R., Wiehe, K., Weissman, D., Pardi, N., Golding, H., Khurana, S., Acharya, P., Andersen, H., Lewis, M. G., Moore, I. N., Montefiori, D. C., Baric, R. S., and Haynes, F. G. (2021) Neutralizing antibody vaccine for pandemic and pre-emergent coronaviruses. *Nature 594*, 553.
(23) Tan, T. K., Rijal, P., Rahikainen, R., Keeble, A. H., Schimanski, L., Hussain, S., Harvey, R., Hayes, J. W. P., Edwards, J. C., McLean, R. K., Martini, V., Pedrera, M., Thakur, N., Conceicao, C., Dietrich, I., Shelton, H., Ludi, A., Wilsden, G., Browning, C., Zagrajek, A. K., Bialy, D., Bhat, S., Stevenson-Leggett, P., Hollinghurst, P., Tully, M., Moffat, K., Chiu, C., Waters, R., Gray, A., Azhar, M., Mioulet, V., Newman, J., Asfor, A. S., Burman, A., Crossley, S., Hammond, J. A., Tchilian, E., Charleston, B., Bailey, D., Tuthill, T. J., Graham, S. P., Duyvesteyn, H. M. E., Malinauskas, T., Huo, J., Tree, J. A., Buttigieg, K. R., Owens, R. J., Carroll, M. W., Daniels, R. S., McCauley, J. W., Stuart, D. I., Huang, K.-Y. A., Howarth, M., and Townsend, A. R. (2021) A COVID-19 vaccine candidate using SpyCatcher multimerization of the SARS-CoV-2 spike protein receptor-binding domain induces potent neutralising antibody responses. *Nat. Commun. 12*, 542.
(24) Kang, Y. F., Sun, C., Zhuang, Z., Yuan, R. Y., Zheng, Q., Li, J. P., Zhou, P. P., Chen, X. C., Liu, Z., Zhang, X., Yu, X. H., Kong, X. W., Zhu, Q. Y., Zhong, Q., Xu, M., Zhong, N. S., Zeng, Y. X., Feng, G. K., Ke, C., Zhao, J. C., and Zeng, M. S. (2021) Rapid Development of SARS-CoV-2 Spike Protein Receptor-Binding Domain Self-Assembled Nanoparticle Vaccine Candidates. *ACS Nano 15*, 2738−2752.
(25) International Clinical Trials Registry Platform. Identifier RPCEC00000340. Phase I study, open, sequential and adaptive for evaluating the safety, reactogenicity and explore the immunogenicity of the prophylactic Vaccine Candidate FINLAY-FR-2 anti SARS-CoV-2 (COVID-19). https://rpcec.sld.cu/en/trials/RPCEC00000340-En.
(26) Betancourt, L. H., Espinosa, L. A., Ramos, Y., Bequet-Romero, M., Rodríguez, E. N., Sánchez, A., Marko-Varga, G., González, L. J., and Besada, V. (2020) Targeting hydrophilic regions of recombinant proteins by MS using in-solution buffer-free trypsin digestion. *Eur. J. Mass Spectrom. 26*, 230−237.
(27) Verez-Bencomo, V., Fernandez-Santana, V., Hardy, E., Toledo, M. E., Rodriguez, M. C., Heynngnezz, L., Rodriguez, A., Baly, A., Herrera, L., Izquierdo, M., Villar, A., Valdes, Y., Cosme, K., Deler, M. L., Montane, M., Garcia, E., Ramos, A., Aguilar, A., Medina, E., Torano, G., Sosa, I., Hernandez, I., Martinez, R., Muzachio, A., Carmenates, A., Costa, L., Cardoso, F., Campa, C., Diaz, M., and Roy, R. (2004) A synthetic conjugate polysaccharide vaccine against Haemophilus influenzae type b. *Science 305*, 522−525.
(28) Dotres, C. P., Puga, R., Ricardo, Y., Brono, C. R., Paredes, B., Echemendia, V., Rosell, S., Gonzalez, N., Garcia-Rivera, D., Valdes, Y., Goldblatt, D., and Verez-Bencomo, V. (2014) Laboratory-Pneumococci Group, Havana-Pneumococci Group Safety and preliminary immunogenicity of Cuban pneumococcal conjugate vaccine candidate in healthy children: a randomized phase I clinical trial. *Vaccine 32*, 5266−5270.
(29) van der Put, R. M. F., Kim, T. H., Guerreiro, C., Thouron, F., Hoogerhout, P., Sansonetti, P. J., Westdijk, J., Stork, M., Phalipon, A., and Mulard, L. A. (2016) A Synthetic Carbohydrate Conjugate Vaccine Candidate against Shigellosis: Improved Bioconjugation and

Impact of Alum on Immunogenicity. *Bioconjugate Chem.* 27 (4), 883−892.
(30) Dalal, J., Rana, R., Harale, K., Hanif, S., Kumar, N., Singh, D., and Chhikara, M. K. (2019) Development and pre-clinical evaluation of a synthetic oligosaccharide protein conjugate vaccine against Neisseria meningitidis serogroup C. *Vaccine 37*, 5297−5306.
(31) Cohen, D., Atsmon, J., Artaud, C., Meron-Sudai, S., Gougeon, M.-L., Bialik, A., Goren, S., Asato, V., Ariel-Cohen, O., Reizis, A., Dorman, A., Hoitink, C. W G, Westdijk, J., Ashkenazi, S., Sansonetti, P., Mulard, L. A, and Phalipon, A. (2021) Safety and immunogenicity of a synthetic carbohydrate conjugate vaccine against Shigella flexneri 2a in healthy adult volunteers: a phase 1, dose-escalating, single-blind, randomised, placebo-controlled study. *Lancet Infect. Dis. 21*, 546−558.
(32) Pichichero, M. E. (2013) Protein carriers of conjugate vaccines: characteristics, development, and clinical trials. *Hum. Vaccines Immunother. 9*, 2505−2523.
(33) Goldblatt, D., Vaz, A. R., and Miller, E. (1998) Antibody avidity as a surrogate marker of successful priming by Haemophilus influenzae type b conjugate vaccines following infant immunization. *J. Infect. Dis. 177*, 1112−1115.
(34) Bingham, K. (2021) The UK Government's vaccine taskforce: strategy for protecting the UK and the world. *Lancet 397*, 68−70.
(35) Hilmer, S., Petrovic, M., Couteur, D. L., Schwartz, J., and Thuermann, P. Geriatric Principles for evaluation and use of COVID-19 vaccines in older adults. Subcommittee of the Clinical Division of IUPHAR (International Union of Basic and Clinical Pharmacology). https://iuphar.org/wp-content/uploads/2021/02/Vaccine-evaluation-for-older-adults_Feb-5.pdf (Accessed on June 13, 2021).
(36) McMahan, K., Yu, J., Mercado, N. B., Loos, C., Tostanoski, L. H., Chandrashekar, A., Liu, J., Peter, L., Atyeo, C., Zhu, A., Bondzie, E. A., Dagotto, G., Gebre, M. S., Jacob-Dolan, C., Li, Z., Nampanya, F., Patel, S., Pessaint, L., Van Ry, A., Blade, K., Yalley-Ogunro, J., Cabus, M., Brown, R., Cook, A., Teow, E., Andersen, H., Lewis, M. G., Lauffenburger, D. A., Alter, G., and Barouch, D. H. (2021) Correlates of protection against SARS-CoV-2 in rhesus macaques. *Nature 590*, 630−634.
(37) Tan, C. W., Chia, W. N., Qin, X., Liu, P., Chen, M. I. C., Tiu, C., Hu, Z., Chen, V. C.-W., Young, B. E., Sia, W. R., Tan, Y.-J., Foo, R., Yi, Y., Lye, D. C., Anderson, D. E., and Wang, L.-F. (2020) A SARS-CoV-2 surrogate virus neutralization test based on antibody-mediated blockage of ACE2−spike protein−protein interaction. *Nat. Biotechnol. 38*, 1073−1078.
(38) Manenti, A., Maggetti, M., Casa, E., Martinuzzi, D., Torelli, A., Trombetta, C. M., Marchi, S., and Montomoli, E. (2020) Evaluation of SARS-CoV-2 neutralizing antibodies using a CPE-based colorimetric live virus micro-neutralization assay in human serum samples. *J. Med. Virol. 92*, 2096−2104.
(39) International Clinical Trials Registry Platform. Identifier RPCEC00000347 Phase II study, multicenter and adaptive for evaluating the immunogenicity, safety and reactogenicity of the Anti-SARS Prophylactic Vaccine Candidate - CoV - 2, FINLAY- FR-2 (COVID-19). https://rpcec.sld.cu/en/trials/RPCEC00000347-En.
(40) International Clinical Trials Registry Platform. Identifier RPCEC00000354 Phase III clinical trial, multicenter, adaptive, parallel-group, randomized, placebo-controlled, double-blind study to evaluate the efficacy, safety and immunogenicity of vaccination against SARS-CoV-2 with 2 doses of FINLAY-FR-2 and a heterologous scheme with 2 doses of FINLAY-FR-2 and a booster dose with FINLAY-FR-1A (COVID-19). https://rpcec.sld.cu/en/trials/RPCEC00000354-En.
(41) Lowry, O. H., Rosebrough, N. J., Farr, A. L., and Randall, R. J. (1951) Protein measurement with the Folin phenol reagent. *J. Biol. Chem. 193*, 265−275.
(42) Ellman, G. L. (1958) A colorimetric method for determining low concentrations of mercaptans. *Arch. Biochem. Biophys. 74*, 443−450.

https://doi.org/10.1021/acschembio.1c00272
ACS Chem. Biol. 2021, 16, 1223−1233